Electrokinetic Delivery of Reactants: Pore Water Chemistry Controls Transport, Mixing, and Degradation

Electrokinetic delivery of reactants: pore water chemistry controls transport, mixing and degradation

Riccardo Sprocati[1], Andrea Gallo[2], Rajandrea Sethi[2], Massimo Rolle[1*]

[1]Department of Environmental Engineering, Technical University of Denmark, Bygningstorvet, Building 115, 2800 Kgs. Lyngby, Denmark

[2]Department of Environmental, Land and Infrastructure Engineering, Politecnico di Torino, Corso Duca degli Abruzzi 24, 10129 Torino, Italy

[*]Corresponding author phone: +45 45251566; email: masro@env.dtu.dk

Abstract

Electrokinetics in porous media entails complex transport processes occurring upon the establishment of electric potential gradients, with a wide spectrum of environmental applications ranging from remediation of contaminated sites to biotechnology. The resulting electric forces cause the movement of pore water ions in opposite directions, leading to charge interactions that can affect the distribution of charged species in the domain. Here, we demonstrate that changes in chemical conditions, such as the concentration of a background electrolyte in the pore water of a saturated porous medium, exert a key control on the macroscopic transport of charged tracers and reactants. The difference in concentration between the background electrolyte and an injected solute can limit or enhance the reactant delivery, cause non-intuitive patterns of concentration distribution, and ultimately control mixing and degradation kinetics. With non-reactive and reactive electrokinetic transport experiments combined with process-based modeling, we show that microscopic charge interactions in the pore water play a crucial role on the transport of injected plumes and on the mechanisms and rate of both physical and chemical processes at larger, macroscopic scales. Our results have important implications on electrokinetic transport in porous media and may greatly impact injection and delivery strategies in a wide range of applications, including in situ remediation of soil and groundwater.

Keywords

Electrokinetic remediation; Porous media; Charge interactions; Reactive transport; Mixing

Introduction

Electrokinetics in porous media has important applications in many different disciplines, as well as an enormous and yet unexplored potential. For instance, electrokinetics (EK) is used in microbial fuel cells[1–3], rapid tests of rocks and concrete[4,5], water purification[6–9] and may play an important role on enhanced and sustainable resources recovery[10–12]. An important environmental application of electrokinetic techniques is the remediation of soil and subsurface porous media[13–15], in which the use of low-intensity electric fields can lead to the mobilization of contaminants and to the effective delivery of reactants and amendments, including bacteria[16–19]. Particularly promising is the capability of electrokinetic processes to distribute reactants in impervious, low-permeability porous media, which are not accessible by hydraulic flushing and can represent long term sources of contamination for soils and groundwater resources[20–22]. An important feature for many subsurface applications is that EK empowers effective delivery and mobilization strategies through the transport mechanisms induced by the application of an electric potential gradient. Such mechanisms include electromigration, consisting in the movement of ions in opposite directions depending on their charge, electroosmosis, resulting in an advective flow caused by the movement of ions in proximity of the solid grains' surfaces, and electrophoresis, affecting the transport of charged particles[23]. Despite the large number of current and potential applications, the quantitative understanding of electrokinetic phenomena in porous media remains a daunting challenge due to the complexity of the controlling processes that depend on physical, chemical and electrical properties of both fluids and solid matrices.

Here, we focus on electromigration transport of charged solutes in saturated porous media and we experimentally demonstrate that the electrolyte composition of the pore water greatly impacts the macroscopic dynamics of electrokinetic transport. We consider permanganate (MnO_4^-) as a colored charged tracer due to its visible properties and its widespread use as strong

oxidant for the degradation of organic contaminants also in EK applications[24–27]. We show that background electrolyte concentrations control the delivery of the injected MnO_4^-, its spatial distribution and its mixing behavior with the surrounding pore water. Furthermore, in our experiments we study reactive transport of MnO_4^-, oxidizing a non-charged organic solute initially present in the porous domain. We illustrate the mechanism and impact of electrokinetically-induced charge mixing, in which the concentration of the background electrolyte affects both the extent of mixing and the kinetics of the mixing-controlled reaction. The electrokinetic experiments are compared with transport by advection and dispersion: the radically different dynamics of EK-induced transport and electrolyte-controlled reactions are systematically analyzed with the support of process-based numerical simulations.

Materials and Methods

To evaluate the displacement mechanisms of a tracer under different conditions of advective-dispersive and electrokinetic transport and to illuminate the role of charge interactions, we designed a quasi-two-dimensional experimental setup, schematically illustrated in Figure S1a-b (Supporting Information). The system consists of a tempered glass chamber (inner size 795 mm × 182 mm × 11 mm) held by an aluminum structure with an internal polyethylene layer. The porous medium (glass beads, with grain size 0.40-0.60 mm, Sigmund Lindner, Germany) was included in the central part of the system (300 mm × 180 mm × 11 mm), delimited by two acrylic separators with honeycomb mesh and covered by a fabric layer.

For the advection-dispersion experiments (Figure S1a), recirculation between the reservoirs was established to ensure the desired hydraulic gradient. The flow rate was controlled with a high-precision, multi-channel peristaltic pump (ColeParmer, United States), and steady-state conditions could be reached in few minutes. The pump was operated with 5 channels, providing a constant seepage velocity in the porous medium of 6.5 cm/h.

For the EK experiments (Figure S1b), graphite rod electrodes (ø6×300 mm, Elektrokul, Denmark) were placed in the glass chamber, in two reservoir zones outside the porous medium. The distance between the two electrodes was 400 mm for all experiments. An electrolyte solution was recirculated in two external reservoirs to provide additional volume to reduce the impact of electrolysis reactions on the system pH. To recirculate water in the reservoirs, a four-channel peristaltic pump (Ole Dich, Denmark) was operated with 2 channels, providing a constant flowrate of 40 mL/min. The graphite electrodes were connected to a power supply (EA Elektro-Automatik, EA-PSI 5200-10A, Germany) by means of electric wires. The voltage provided by the power supply throughout the experiments was kept constant at 200 V. The current in the system was measured by connecting the wire from the power supply to the anode through a multimeter (PeakTech 3315, Germany). The effective potential drop within the porous media was measured by means of two wire electrodes (exposed tip 2 mm) placed centered in the setup, 10 mm below the water table and at a distance of 280 mm. The potential reading was performed with a second digital multimeter (PeakTech 3315, Germany). Voltage and current measurements were recorded with the multimeter at every hour of operation and were found to be in a range 122.1-148.7 V and 3.0-24.8 mA, respectively. The values measured in the different experiments are reported in the Supporting Information (Table S1).

Advection-dispersion and EK transport have been studied performing injections of potassium permanganate ($KMnO_4$) on the left-side of the domain. To investigate the role of charge interactions on the transport of ions, we performed first a set of conservative, non-reactive experiments followed by a second set of reactive experiments, in which glucose (Sigma-Aldrich, United States) was added to the background solutions to reach a concentration of 8 mol/m^3. For all experiments, the concentration of the injected $KMnO_4$ was constant (3 mol/m^3) whereas the background electrolyte concentration, consisting in a solution with a fixed ratio of $NaHCO_3$ and Na_2CO_3 to reach a pH of 9, was varied for the different investigated scenarios.

In all cases, the injected tracer solution displaces the background fluid and creates a circular plume shape and a conductivity difference in the system.

The experiments were conducted in a dark room and the glass chamber was illuminated from the back with an electroluminescent panel (1000 mm × 300 mm, EL-Technik, Germany) and from the front with a light bulb (Philips 4000K, 806 lm, 100 mA, 9.5W). A calibration procedure was developed to relate the color intensity of permanganate with its concentration and to quantify the spatial distribution of the permanganate plumes in the porous medium at different times. Details about the setup and the image analysis and calibration techniques are provided in Supporting Information (Section S2).

Theoretical background

The transport of dissolved species in saturated porous media occurs as a result of concentration, electric potential and pressure gradients. These phenomena result in diffusion/dispersion, electromigration and advective fluxes, which are described by the Nernst-Planck equation[28–33]:

$$\boldsymbol{J}_i^{Tot} = \underbrace{-nD_i\nabla c_i}_{\boldsymbol{J}_i^{Dif}} \underbrace{-nD_i\frac{z_iF}{RT}c_i\nabla\Phi}_{\boldsymbol{J}_i^{Mig}} \underbrace{+n\boldsymbol{u}c_i}_{\boldsymbol{J}_i^{Adv}} \quad (1)$$

where n is the porosity, c_i is the molar concentration, D_i is the pore diffusion/dispersion coefficient, z_i is the charge number, Φ is the electric potential and $\boldsymbol{u}$ is the seepage velocity.

In absence of advective fluxes, transport by electromigration, provided sufficient electric potential gradients, is the dominant component. Such situation is typical of electrokinetic applications, in which the transport of ions by electromigration depends on the applied electric potential, on the diffusive/dispersive properties and on the charge of the individual ions. This makes anions and cations move in presence of an electric field in opposite directions, whereas non-charged solutes are not affected by the applied voltage. Considering a porous medium, ions in solution need to comply with the electroneutrality condition $\sum_{i=1}^{N} z_i c_i = 0$, which

corresponds to the Poisson's equation under the assumption of overall zero charge density in the domain[34,35]. Given that ions in aqueous solutions have different diffusion coefficients (Table S3, Supporting Information), under the application of an electric field they will move with different electromigration velocities. Such properties, in combination with the electroneutrality condition, imply that the electrokinetic transport of ions is affected by the overall electrolyte composition of the system, thus making charge interactions play a key role for the movement of the different charged species.

Considering that the application of an electric current in a porous medium results in a flux of ions, it is possible to define the current density from the definition of total fluxes in Eq. 1. As an external current can result in significant electric potential gradients, it is possible to assume that the current density can be approximated as[28]:

$$\boldsymbol{I} = F\sum_{i=1}^{N} J_i^{Mig} z_i = F^2 \sum_{i=1}^{N} z_i^2 \frac{nD_i}{RT} c_i \nabla\Phi = \sigma_e \nabla\Phi \qquad (2)$$

Eq. 2 indicates that there are strong dependencies between the current density I and the conductivity of the electrolyte solution σ_e. In particular, as σ_e changes in the system, the current density and the electric potential gradient are also spatially and temporally variable in the porous medium domain. Indeed, changes in electric potential gradients impact the intensity and direction of migration fluxes, which ultimately affect the concentration and distribution of ionic species in the system.

Process-based numerical modeling was performed with the codes NP-Phreeqc[36] and NP-Phreeqc-EK[37] for the cases of advection-dispersion and electrokinetic transport, respectively. These simulators are based on a coupling between COMSOL Multiphysics and the geochemical code PhreeqcRM[38], operated through a MATLAB LiveLink interface. For electrokinetic transport, NP-Phreeqc-EK solves the Nernst-Planck-Poisson equations in multidimensional domains and is able to account for a wide range of equilibrium and

kinetically-controlled reactions. The coupling with the geochemical code accounts for the composition and aqueous speciation of the pore water. The initial solution speciation for each scenarios is reported in Tables S4 (Supporting Information).

Results and discussion

Conservative transport experiments

For the set of conservative experiments, the first scenario focuses on the movement of the purple-colored permanganate ion (MnO_4^-) undergoing advective-dispersive transport induced by a simple pressure head gradient and without applying any electric potential difference between the electrodes (Figure 1). Three experimental scenarios were then dedicated to the investigation of EK transport. In these experiments, the application of a constant electric potential at the electrodes resulted in transport of the injected permanganate by electromigration. The electric potential in the system was set to provide an electromigration velocity comparable with the seepage velocity in the advective-dispersive experiment. Therefore, the electromigration velocity of MnO_4^- in the system was approximately 6.5 cm/h. The considered EK transport scenarios were characterized by three different electrolyte concentrations of the background pore water solution. We refer to “EK equal” for the scenario in which the sum of all cations (or anions) in the pore water is equal to the one of the injected $KMnO_4$ solution. Scenarios “EK low” and “EK high” represent situations in which the sum of cation equivalents in the background electrolyte solution is, respectively, three times lower and three times higher than the concentration of the injected tracer. Upon application of an electric field, the anions (including permanganate) move towards the anode on the right, whereas the cations are transported towards the cathode on the left. Figure 1a shows a sketch of the experimental setup and summarizes the injection and pore water concentrations in the different experiments.

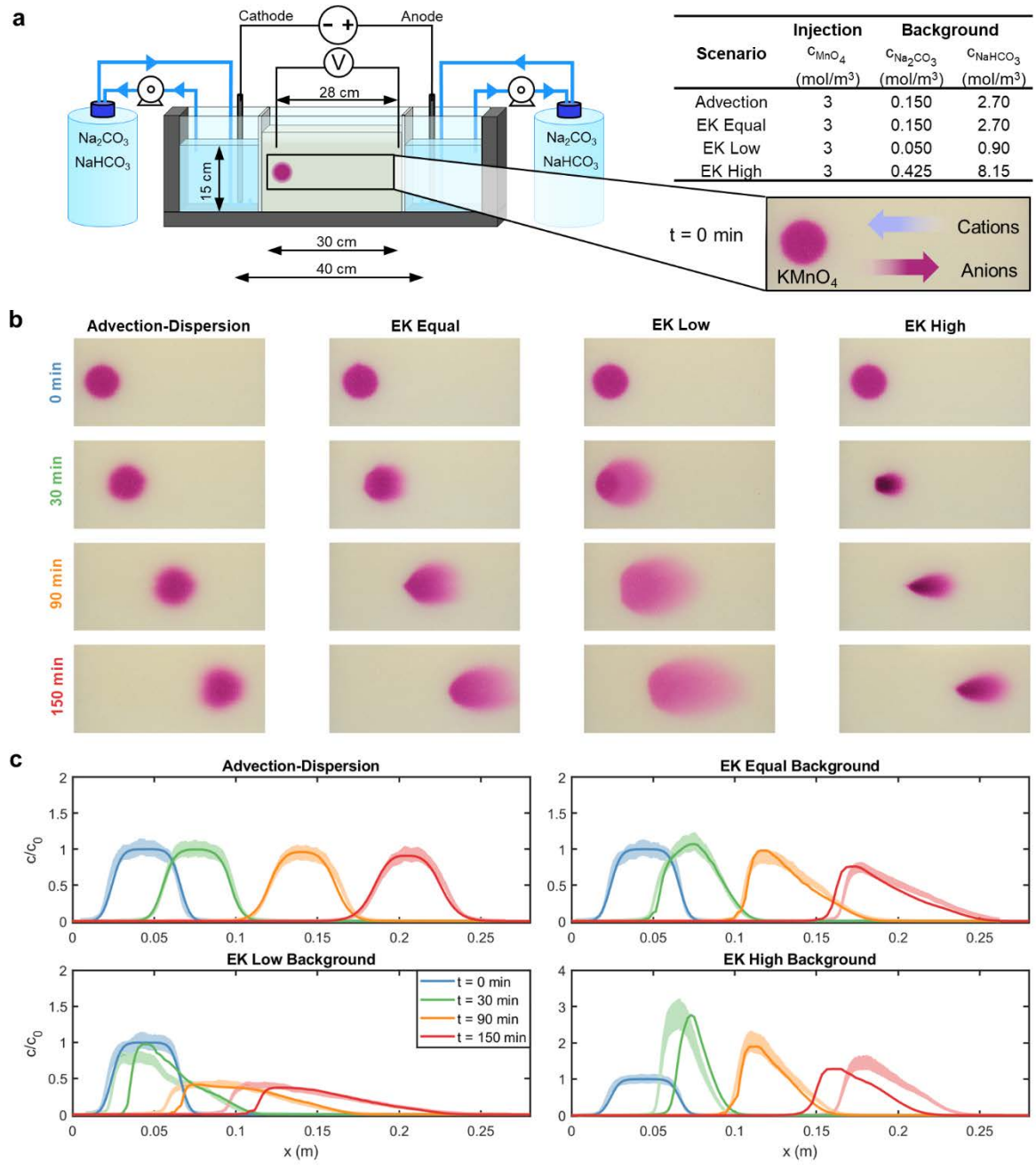

Scenario	Injection c_{MnO_4} (mol/m³)	Background $c_{Na_2CO_3}$ (mol/m³)	Background c_{NaHCO_3} (mol/m³)
Advection	3	0.150	2.70
EK Equal	3	0.150	2.70
EK Low	3	0.050	0.90
EK High	3	0.425	8.15

Figure 1. ***a*** *Illustration of the experimental setup and summary of concentrations used in the different experiments.* ***b*** *images showing the evolution of the permanganate plume in the four different experiments.* ***c*** *concentration profiles evaluated through the longitudinal axis of the permanganate plume. The shaded area represents the experimental observations relating color intensity to concentration including uncertainty bands (±2σ), whereas the solid lines are the simulation outcomes.*

For every scenario we monitored the evolution of the tracer plume in the porous medium by collecting pictures every minute for 150 minutes; Figure 1b presents four successive images of each experiment. Considering the advection-dispersion case, the permanganate plume has a regular and symmetric shape and moves with the water at the average linear pore water velocity. Conversely, in the EK transport cases, although the nominal migration velocity is comparable to the average pore water velocity in the advection-dispersion case, the shapes are very different and the plumes appear to be substantially deformed with respect to the initial circular shape. For instance, in scenario "EK equal", the permanganate plume becomes elongated and a smooth concentration gradient develops at the front. A similar but more pronounced behavior is observed for scenario "EK low", in which the permanganate plume has a lower color intensity and is significantly more stretched in the longitudinal and transverse directions. In contrast, in scenario "EK high", the permanganate plume initially contracts and assumes a darker color. Successively, as the plume migrates towards the anode, it develops an elongated shape parallel to the applied electric field. The velocity of plume displacement for "EK equal" and "EK high" is similar and comparable with the advection-dispersion scenario. In these cases, the center of mass of the plume has traveled a distance of approximately 150 mm after 150 min. The small electrolyte concentration in the case "EK low" has a clear effect of retarding the plume. After 150 min and despite the application of the same electric potential gradient, the centroid of the "EK low" plume has covered only 2/3 of the distance (~100 mm) of the other plumes.

Figure 1c illustrates the longitudinal profiles of the MnO_4^- concentrations at different times. Such profiles were evaluated both from the pictures, using a calibration function relating the color intensity to the tracer concentration, and from the outcomes of a 2-D forward model, describing the physical and electrostatic processes in the setup[36,37,39]. The simulation results,

showing the two-dimensional spatial distribution of the permanganate plumes at the different times, are presented in Figure S4. In the first experimental scenario, with transport induced by the hydraulic gradient, the permanganate concentration profiles are regular and follow the classic theory of transport in porous media[40], as shown by the good agreement of the experimental observations with the advection-dispersion simulations (Figure 1c). The transport becomes radically different when MnO_4^- is displaced by electromigration. For instance, in the "EK equal" experiment, the plume develops a smoother concentration front, whereas the back of the plume presents a steep concentration profile even at late times. This behavior, inherently dissimilar from advective-dispersive transport, can be simulated considering the charge interactions and the coupled Nernst-Planck fluxes of the different charged species in the domain.

The results of the numerical simulations allowed us to reproduce the experimental observations very well, including the concentration values as well as the shape and the evolution of the permanganate plume in the setup. In the scenario "EK low", the permanganate plume starts to expand and slowly displaces with a lower concentration with respect to the previous scenarios. The peak concentration (~1 mol/m^3) is in the order of the low background electrolyte concentration in the pore water. Both the pictures and the longitudinal profiles also clearly show a slower movement of the permanganate plume compared to the other experimental scenarios. Conversely, in the scenario with high electrolyte background ("EK high"), the concentration of the permanganate plume initially increases, with the highest value almost three times the injected concentration. Successively, the plume migrates towards the anode with similar velocity and smooth concentration fronts as in the scenario "EK equal".

Charge interaction mechanisms

Process-based numerical modeling is essential to mathematically describe electrokinetic transport mechanisms, to visualize the spatial distribution of the delivered and of the background charged species, to illuminate their coupled displacement and, ultimately, to allow a quantitative interpretation of the experimental observations.

Figure 2a presents the simulated longitudinal concentration profiles of the different ions in the experimental setup at the initial time and after 90 minutes. In the EK scenario with equal background, MnO_4^- moves towards the anode, whereas K^+ exits the porous medium to the cathode reservoir. In such scenario, the major background ions (sodium and bicarbonate) are uniformly present in the domain at the beginning of the experiment, except in the area where they were displaced by the injected $KMnO_4$ solution. Upon application of the electric potential, HCO_3^- is transported towards the anode, in the same direction of MnO_4^-. At the same time, the major cation in the system, Na^+, moves in the opposite direction towards the cathode. Note that in every point, due to the condition of electroneutrality, the sum of equivalents of both cations and anions must be the same. Consequently, the shape of the profiles of MnO_4^- and HCO_3^- appear to be complementary as one anion can replace the other although together they cannot exceed the charge that is carried by the cations in the same location. The smooth front of MnO_4^- and the low concentration of HCO_3^- are mainly due to their different aqueous diffusion coefficients (i.e., 1.50×10^{-9} for MnO_4^- and 1.09×10^{-9} for HCO_3^-). The higher diffusivity of MnO_4^-, leads to its faster transport. However, such tendency is slowed down by the coupling with HCO_3^-, which needs to be displaced and the overall charge in the system has to be balanced. As a result, only a fraction of the permanganate front is able to proceed at the nominal electromigration velocity imposed by the voltage difference at the electrodes, thus resulting in a smooth front progressively advancing in the domain.

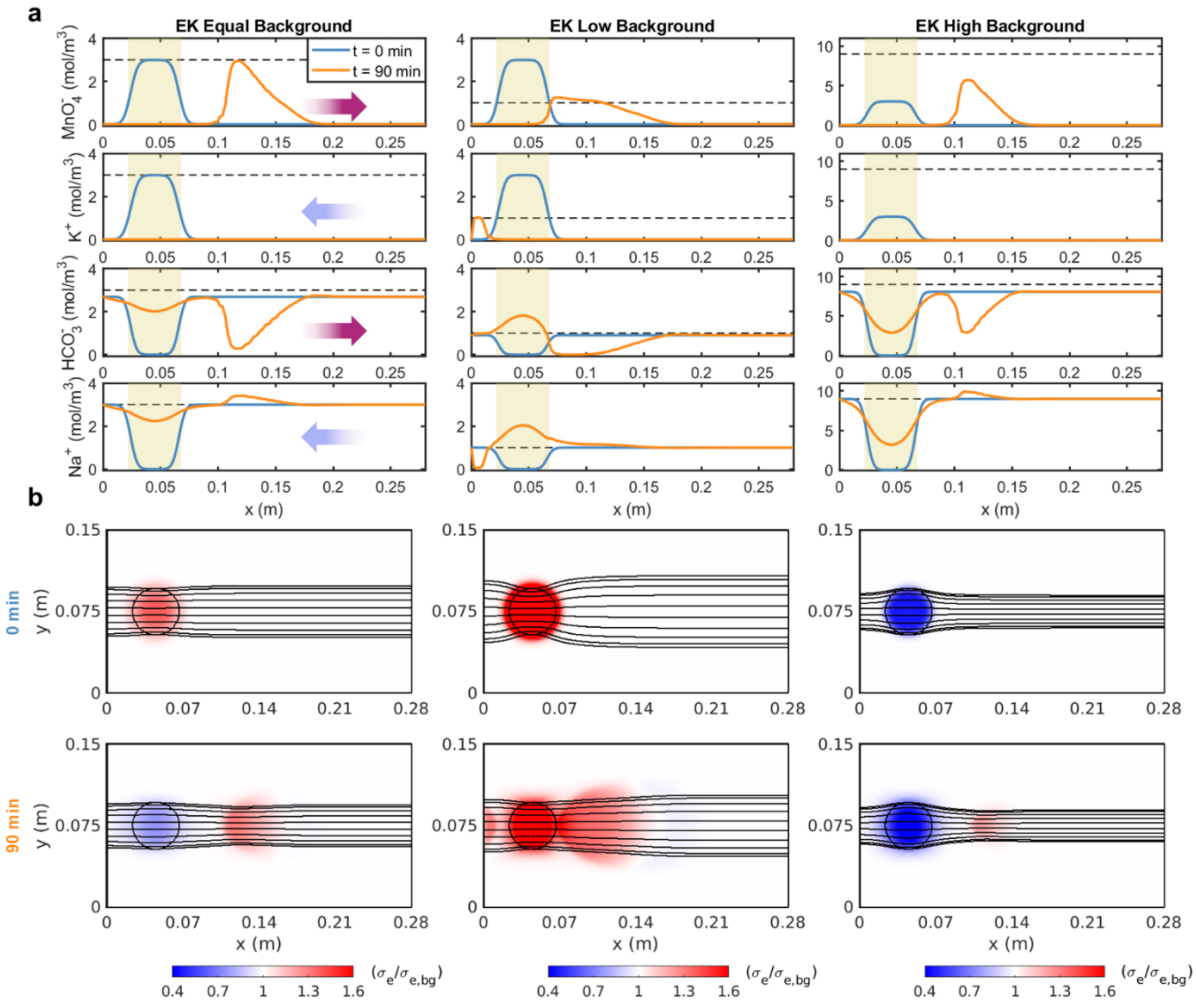

Figure 2*. Simulated concentrations of major cations (Na^+ and K^+), anions (HCO_3^- and MnO_4^-) in the pore water and 2D electrolyte conductivity at different times.* ***a*** *cross-section illustrating the transport of the major ions in the system a t=0 and t=90 minutes for all three EK scenarios. The dashed lines represent the sum of all positive or negative charge equivalents in the system whereas the shaded area indicates the initial zone where the tracer has been injected.* ***b*** *normalized electrolyte conductivity maps with respect to the background conductivity for the three EK scenarios at t=0 and t=90 minutes (upper and bottom rows, respectively). The lines are the computed electric field streamlines passing through the central zone of the porous medium, where the tracer was injected.*

In the experiment with lower background ("EK low"), the concentration of MnO_4^- during transport decreases significantly and approaches the values corresponding to the sum of the equivalents of all cations in the background solution (dashed line in Figure 2a). This is the result of the lower concentration of cations in the pore water, which limits the delivery of permanganate. Only a fraction of the injected plume can enter the volume initially occupied by the background electrolyte and starts to move towards the anode. The concentrations of Na^+ and HCO_3^- in the injection zone increases to fulfil the charge balance in this portion of the domain where higher amounts of K^+ and MnO_4^- were initially injected. Finally, in the experimental scenario with high background electrolyte ("EK high"), the increase of permanganate concentration is the result of the high Na^+ present in the background (moving towards the cathode), which requires a higher concentration of MnO_4^- (moving towards the anode) to comply with the condition of electroneutrality. In this scenario, also the concentration of both Na^+ and HCO_3^- after 90 minutes in the initial area of injection is similar to the initial concentration of K^+ and MnO_4^-. Such situation is particularly interesting since the increase in concentration, caused by electromigration fluxes (Figure S5) and resulting from the charge interactions in the multicomponent ionic system, occurs against the natural concentration gradient (Figure S6).

These experiments clearly show that the background electrolyte concentration controls the mechanisms of electrokinetic transport and, thus, the delivery, the shape and the evolution of the injected permanganate plumes. The driving force is indeed the electric potential gradient in the system, which in turn is influenced by the electrolyte conductivity. The latter is a spatially variable quantity in the considered setup, as illustrated in Figure 2b for all EK scenarios at t=0 and t=90 minutes. In scenario "EK equal", despite the concentrations of the background and the tracer solutions are the same, the conductivity of the injected $KMnO_4$ plume is higher as a result of the higher diffusivity of MnO_4^- and K^+ compared to the background ions. After 90

minutes, the distribution of MnO_4^- can be directly related to the electrolyte conductivity map with a higher σ_e, whereas the injection zone still shows a lower value of σ_e due to the lower diffusion coefficients of the background ions that occupied the injection's pore space. At this later time, also the electric field streamlines are different and appear to focus on the area of the permanganate plume, which has higher σ_e and has moved towards the anode. Similarly, in the scenario with low background concentration, a strong focusing of the streamlines occurs in the zone with initial injection of the plume where the higher σ_e results from the higher concentration of the injected permanganate solution with respect to the background. This phenomenon is due to the focusing of the electric field streamlines in zones with higher electrolyte conductivity, where the intensity of the electric field is higher. Also in this case, a subsequent defocusing of the streamlines causes a larger spreading of the permanganate plume. At later times, the progressive distribution of the mass from the initial injection and the limiting effect of the background electrolyte concentrations tend to suppress the differences in conductivity.

For the scenario with high background electrolyte concentration, the streamlines show an opposite pattern, first defocusing in the injection zone (low σ_e) and then focusing in the direction of permanganate transport. In this case, it is possible to observe an increase of σ_e as a result of the progressive increase in MnO_4^- concentration, as the permanganate plume shrinks during its displacement towards the anode.

Overall, the computed 2D maps of electrolyte conductivity illustrate the evolution of this property in the domain and the effects on the electric potential streamline patterns, which directly affect the observed shape and propagation of the permanganate plume in the experimental setup. Interestingly, during EK also the initial conditions of the system such as local differences in σ_e between the injected tracer solution and the background are maintained at later times and such effects only dissipate slowly as a result of diffusion.

Plume spreading and mixing

Transport of solutes in porous media results from complex pore-scale flow and mass transfer processes that determine the macroscopic shape and evolution of injected plumes. Metrics allowing the quantification of plume spreading and mixing are essential to describe solute transport in porous domains[41,42]. The second central spatial moments, quantifying the mean displacement of the concentration distribution from the plume centroid, are typically evaluated to characterize plume spreading[43]. Here we determine the moments of the permanganate plumes observed in our experiments as well as in the model simulations. To determine plume mixing, instead, we use the concept of the dilution index, a metric based on the Shannon entropy that quantifies the effective volume occupied by the plume[44]. Plume spreading and mixing are evaluated for all conservative scenarios with the equations summarized in the Supporting Information (Section S4). Figure 3a shows the permanganate plumes after 90 minutes from the injection for the four considered experimental scenarios. The pictures clearly show different plume shape, mass distribution and solute concentration resulting from the transport and electrostatic mechanisms in the experiments performed. The longitudinal and transverse second central moments exhibit a distinct behavior in the experiments (Figure 3b). In the advection-dispersion scenario, the longitudinal and transverse moments show a gradual increase due to hydrodynamic dispersion at the plume fringes. In the EK scenario with the same background concentration ("EK equal"), instead, the permanganate plume spreading is larger both in the longitudinal and in the transverse directions. Spreading in both directions is very pronounced in the experiment with low concentration of the background electrolyte in which the observed permanganate concentrations are low and the plume spreads over a large portion of the porous medium. The trends of the computed moments show higher slope at the beginning, indicating that the spreading enhancement is more effective at early times. In the

scenario “EK high”, the plume initially shrinks and then spreads. Such behavior is apparent from the computed moments, showing decreasing values from the initial injection followed by an increase as the plume is displaced towards the anode. The rate of increase is more pronounced in the longitudinal direction, resulting in higher moments at late times compared to the advection-dispersion case. For all the cases, the spatial moments from the 2-D simulations allow capturing the trends computed from the experimental data.

Figure 3*. Metrics of spreading and mixing.* ***a*** *images of the permanganate plumes for the different scenarios at t=90 minutes.* ***b*** *Second central spatial moments, dilution index and peak concentration expressed as a function of time. The solid lines indicate model predictions whereas the shaded areas represent the experimental results.*

Figure 3b also shows the evolution of the dilution index and the peak concentration of the permanganate plumes. Such metrics are intrinsically related[44,45] and quantify the capability of the injected plumes to effectively mix with the background pore water. In the advection-

dispersion case the dilution index shows a mild linear increase, as expected for transport in a two-dimensional homogeneous porous medium, $E \sim t^{n/2}$, where n is the dimensionality of the system[44]. Dilution appears to be stronger in the "EK equal" and "EK low" scenarios. In particular, the latter case exhibits more than double increase in the plume dilution. These results show the capability of EK transport to effectively distribute the mass of the injected tracer over a larger pore water volume. Different, and perhaps even more interesting, is the case "EK high". In such scenario the dilution index shows a non-monotonic trend with an initial decrease (approximately half of the initial value during the first 30 minutes) followed by an increase to a level similar to the dilution of the injected circular plume. The initial trend of the dilution index of the MnO_4^- plume is counterintuitive based only on conventional mass transfer mechanisms, since it indicates that the plume decreases its entropy. However, as explained above, the plume shrinking, the peak concentration increase (almost three times the injected values) and the dilution decrease are due to the electrostatic interactions with the ions present at high concentration in the background pore water electrolyte and to the electroneutrality constraint.

Reactive transport experiments

These experiments explored the displacement and degradation reaction of MnO_4^- under advective-dispersive and electrokinetic transport. Permanganate was delivered in the porous media with a background electrolyte containing glucose (8 mol/m^3) as model organic compound. When these two reactants come into contact an oxidation-reduction reaction occurs, which is described as a bimolecular reaction kinetics. In this set of reactive transport experiments, the same EK scenarios with equal, low and high background concentration of electrolytes were investigated and the results are illustrated in Figure 4.

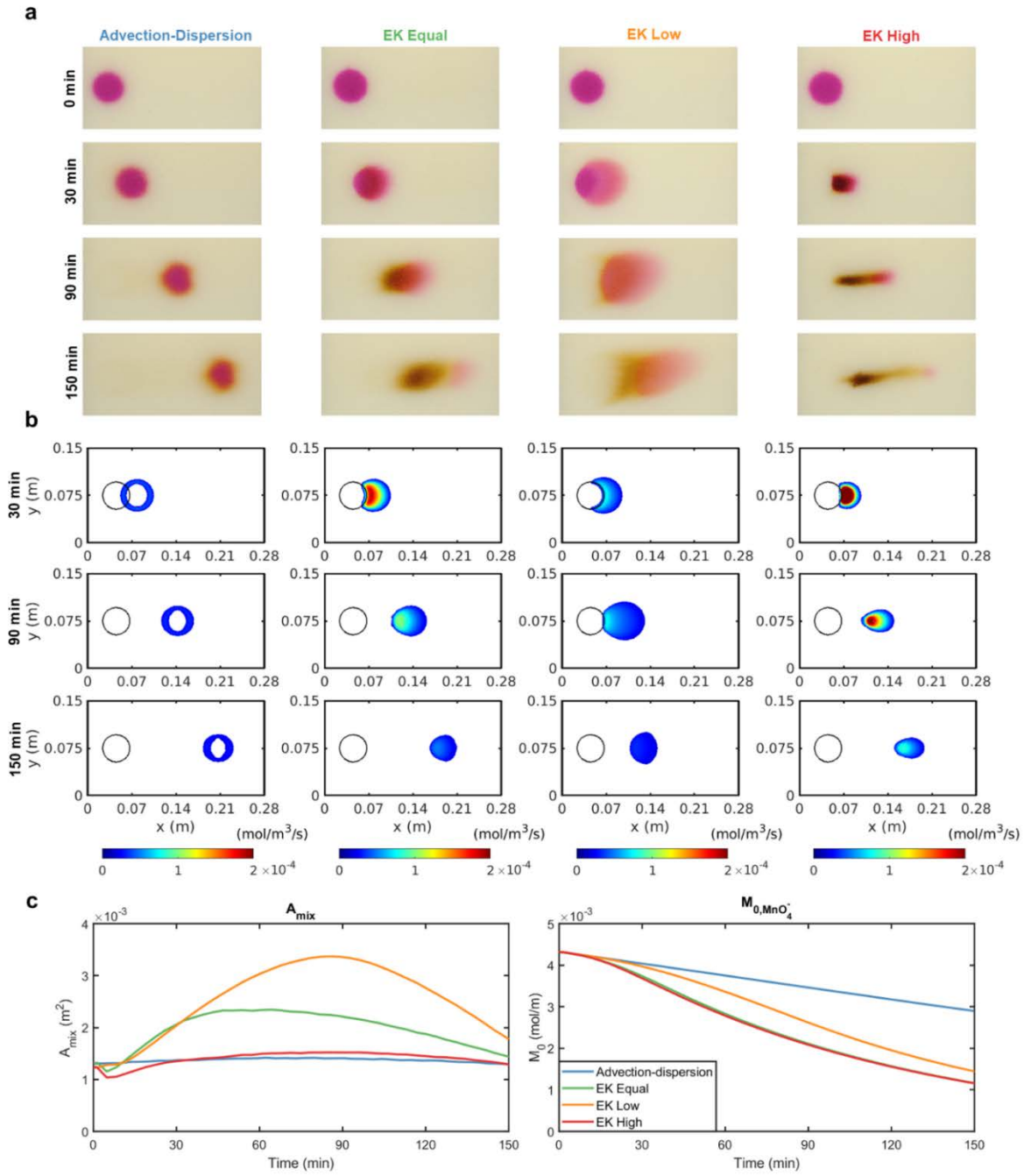

391

392 ***Figure 4***. *Reactive transport experiments and model analysis.* ***a*** *images showing the temporal*
393 *evolution of the reactant plumes.* ***b*** *simulated reaction rates, considering a limiting threshold*
394 *of* 2×10^{-5} *mol/m*^{3}*/s for all scenarios that allows the visualization of the different reaction*
395 *patterns.* ***c*** *evaluation of the area for the mixing-controlled reaction and of the* MnO_4^- *mass*
396 *simulated in the different scenarios.*

397

Figure 4a shows the evolution of the reactive system for the different scenarios over time. In case of advection-dispersion, the reaction occurs at the fringe of the plume, where the permanganate mixes with the glucose in the background pore water by hydrodynamic dispersion. When the two solutes come into contact, the mixing-controlled reaction occurs. The reaction area is visible from the pictures showing the formation of oxidation products at the plume fringe and also from the numerical simulations. In this scenario the reactive fringe moves with the permanganate plume in the same direction of the advective flow (Figure 4b).

In case of EK transport, the mixing mechanisms and the resulting patterns of reactants and products distribution are completely different (Figure 4a-b). The applied electric field causes the displacement of permanganate by electromigration but has no effect on the non-charged glucose. Therefore, the mixing pattern resembles chromatographic mixing with an effective overlap of the displaced permanganate with the immobile organic compound in the pore water. The reactive zone is large, extending to the whole area of the plume, and is not restricted to a thin fringe at the plume boundary. Indeed, in case of EK transport, more extensive degradation and more effective consumption of permanganate are observed. It is also of interest to note the effects of the different background electrolyte concentrations in the distinct EK reactive transport experiments. When the electrolyte background solution has an equal concentration with respect to the injected permanganate, the reaction occurs effectively and, after 150 minutes, almost all MnO_4^- has been consumed. In the case with low background electrolyte concentration, the MnO_4^- plume spreads significantly and its concentration in the porous medium is limited by the background electrolyte. Such behavior results in a large mixing area but in a considerably slower reaction kinetics leading to only partial consumption of the oxidant. Therefore, the slow kinetics of the redox reaction is the overall rate-limiting step, resulting in the presence of a significant permanganate plume even after 150 minutes. Lastly, in the experimental scenario with higher background concentration, the permanganate plume

shrinks and its concentration is increased. The mixing area is smaller but reactive mixing is effective due to the higher concentration of MnO_4^- leading to faster reaction kinetics and to an almost complete consumption of the permanganate plume.

Figure 4b illustrates the spatial and temporal distribution of the mixing-controlled reactive zones in the different scenarios. The evolution of the computed mixing area and of the reaction efficiency, quantified through the computed mass of permanganate in the domain, are shown in Figure 4c. The mixing area is larger in the cases “EK equal” and “EK low” in which permanganate electromigration and the composition of the background electrolyte solution lead to an extended mixing zone. Such area of contact between the reactants reaches a maximum and, successively, starts to decrease due to the consumption of the permanganate plume. The mixing area is considerably more limited in the “Advection-Dispersion” and “EK high” experiments. In these cases the values reached are similar but, as discussed above and illustrated in Figure 4a-b, the shape of the mixing zone is completely different due to the different transport mechanisms. Considering the degradation of the permanganate plumes upon reaction with the glucose in the pore water, the simulations show nonlinear decreasing trends of the remaining mass with significantly higher permanganate consumption in presence of electrokinetic transport. In particular, the cases “EK equal” and “EK high” show the highest efficiency and the lowest mass of permanganate in the system at the end of the simulation. In these cases the simulation outcomes show that 75% of the initial permanganate mass was consumed. A smaller efficiency (70% of the initial mass consumed) characterized the scenario “EK low”, whereas the lowest efficiency was observed in the advection-dispersion case in which only 35% of the initial permanganate mass was consumed.

Implications for electrokinetic applications

Our investigation highlights important aspects and mechanisms of both scientific and practical relevance for electrokinetic transport of charged species in porous media, which is of crucial importance in different disciplines and has a wide range of current and potential applications in geological, environmental, industrial and biological systems. We demonstrate that the pore water chemistry and microscopic Coulombic interactions can both limit and/or enhance the delivery of charged tracers by electrokinetics. The EK transport experiments performed clearly show that when the background concentration of the cations or anions is significantly smaller than an injected charged tracer, the tracer concentration that it possible to deliver by electromigration is limited by the concentration level of the background electrolyte solution. The ionic composition of the pore water also controls the tracer displacement, impacting the movement of the center of mass as well as the shape and spreading of the plume both in longitudinal and lateral directions. Moreover, the dilution of the injected tracer depends on the background electrolyte that, when present at high concentration, can even lead to a decrease of the dilution and the entropy of the plume and to an increase of its peak concentration. Of environmental significance are also the outcomes of the reactive transport experiments showing fascinating aspects of electrokinetically-induced charge species' mixing, leading to different mass removal efficiencies and to quantitatively important effects of the pore water chemistry on the kinetics of mixing-controlled degradation.

This investigation opens interesting perspectives on the possibility to employ microscopic charge interactions to control macroscopic transport and to design innovative delivery strategies in porous media that can be effectively implemented in practical applications, such as soil and groundwater remediation. The mechanistic understanding of the fundamental role of background electrolyte composition for the delivery of charged species during EK and the developed process-based model, will allow the improvement of the performances of electrokinetic distribution techniques for nutrients[39,46–48] and reactants[49–52] in subsurface

porous media. Specific examples include the quantitative assessment of the amounts and distribution of delivered species, the optimization of voltage values, and the planning of delivery strategies such as alternating active/inactive EK phases. Applications for subsurface remediation encompass both low-permeability zones[25,26] but may also be employed to enhance mixing and degradation of contaminant plumes in permeable aquifer systems, where poorly mixing flow and transport regimes and mass transfer limitations[53] represent typical bottlenecks to effective remediation. The detailed process knowledge obtained in this study will also be instrumental for quantitative understanding of electrokinetic transport in heterogeneous porous media, where high spatial variability of physical and chemical properties (e.g., permeability, porosity, surface charge and pore water composition) will affect the electrokinetic delivery of reactants, and where strong interactions between the different electrokinetic transport processes will impact the effectiveness of in situ EK interventions. Finally, the combined experimental and process-based modeling approach proposed in this study could be extended and further developed for the use of different tracers and reactants, including micro- and nanomaterials for subsurface remediation[54,55].

Acknowledgments

The authors would like to acknowledge the support of the Capital Region of Denmark, the H.C. Ørsted Fond and the PhD fellowship at Politecnico di Torino (DIATI Department), as well as the help of Emil Bay Frantzen in the experimental activities. Constructive comments of three anonymous reviewers helped improving the quality of the manuscript.

Associated content

Supporting Information

Details of the experimental setup, image analysis, governing equations, metrics of spreading, dilution and mixing, and numerical modeling approach. 2-D model results of permanganate transport at different times for the four conservative scenarios, simulated 2-D advective and electromigration fluxes and diffusive/dispersive fluxes. Tables summarizing experimental conditions (e.g., voltage, current, pH and temperature) and parameters used for the process-based numerical modeling.

References

(1) Xie, X.; Ye, M.; Hsu, P. C.; Liu, N.; Criddle, C. S.; Cui, Y. Microbial Battery for Efficient Energy Recoèery. *Proc. Natl. Acad. Sci. U. S. A.* **2013**, *110* (40), 15925–15930. https://doi.org/10.1073/pnas.1307327110.

(2) Logan, B. E. Exoelectrogenic Bacteria That Power Microbial Fuel Cells. *Nat. Rev. Microbiol.* **2009**, *7*, 375–381. https://doi.org/10.1038/nrmicro2113.

(3) He, Z.; Minteer, S. D.; Angenent, L. T. Electricity Generation from Artificial Wastewater Using an Upflow Microbial Fuel Cell. *Environ. Sci. Technol.* **2005**, *39* (14), 5262–5267. https://doi.org/10.1021/es0502876.

(4) Friedmann, H.; Amiri, O.; Aït-Mokhtar, A.; Dumargue, P. A Direct Method for Determining Chloride Diffusion Coefficient by Using Migration Test. *Cem. Concr. Res.* **2004**, *34* (11), 1967–1973. https://doi.org/10.1016/j.cemconres.2004.01.009.

(5) Löfgren, M.; Neretnieks, I. Through-Electromigration: A New Method of Investigating Pore Connectivity and Obtaining Formation Factors. *J. Contam. Hydrol.* **2006**, *87* (3–4), 237–252. https://doi.org/10.1016/j.jconhyd.2006.05.006.

(6) Alkhadra, M. A.; Conforti, K. M.; Gao, T.; Tian, H.; Bazant, M. Z. Continuous Separation of Radionuclides from Contaminated Water by Shock Electrodialysis. *Environ. Sci. Technol.* **2019**, *54* (1), 527–536. https://doi.org/10.1021/acs.est.9b05380.

(7) Gabarrón, S.; Gernjak, W.; Valero, F.; Barceló, A.; Petrovic, M.; Rodríguez-Roda, I. Evaluation of Emerging Contaminants in a Drinking Water Treatment Plant Using Electrodialysis Reversal Technology. *J. Hazard. Mater.* **2016**, *309*, 192–201. https://doi.org/10.1016/j.jhazmat.2016.02.015.

(8) Patel, S. K.; Qin, M.; Walker, W. S.; Elimelech, M. Energy Efficiency of Electro-Driven Brackish Water Desalination: Electrodialysis Significantly Outperforms Membrane Capacitive Deionization. *Environ. Sci. Technol.* **2020**, *54* (6), 3663–3677. https://doi.org/10.1021/acs.est.9b07482.

(9) Sun, M.; Qin, M.; Wang, C.; Weng, G.; Huo, M.; Taylor, A. D.; Qu, J.; Elimelech, M. Electrochemical-Osmotic Process for Simultaneous Recovery of Electric Energy, Water, and Metals from Wastewater. *Environ. Sci. Technol.* **2020**, *54*, 8430–8442. https://doi.org/10.1021/acs.est.0c01891.

(10) Martens, E.; Prommer, H.; Dai, X.; Wu, M. Z.; Sun, J.; Breuer, P.; Fourie, A. Feasibility of Electrokinetic in Situ Leaching of Gold. *Hydrometallurgy* **2018**, *175*, 70–78. https://doi.org/10.1016/j.hydromet.2017.10.020.

(11) Guedes, P.; Couto, N.; Ottosen, L. M.; Ribeiro, A. B. Phosphorus Recovery from Sewage Sludge Ash through an Electrodialytic Process. *Waste Manag.* **2014**, *34* (5), 866–892. https://doi.org/10.1016/j.wasman.2014.02.021.

(12) Ribeiro, A. B.; Mateus, E. P.; Ottosen, L. M.; Bech-Nielsen, G. Electrodialytic Removal of Cu, Cr, and As from Chromated Copper Arsenate-Treated Timber Waste. *Environ. Sci. Technol.* **2000**, *34* (5), 784–788. https://doi.org/10.1021/es990442e.

(13) Probstein, R. F.; Hicks, R. E. Removal of Contaminants from Soils by Electric Fields. *Science (80-.).* **1993**, *260* (5107), 498–503. https://doi.org/10.1126/science.260.5107.498.

(14) Acar, Y. B.; Alshawabkeh, A. N. Principles of Electrokinetic Remediation. *Environ. Sci. Technol.* **1993**, *27* (13), 2638–2647. https://doi.org/10.1021/es00049a002.

(15) Cox, C. D.; Shoesmith, M. A.; Ghosh, M. M. Electrokinetic Remediation of Mercury-Contaminated Soils Using Iodine/Iodide Lixiviant. *Environ. Sci. Technol.* **1996**, *30* (6), 1933–1938. https://doi.org/10.1021/es950633r.

(16) Qin, J.; Sun, X.; Liu, Y.; Berthold, T.; Harms, H.; Wick, L. Y. Electrokinetic Control of Bacterial Deposition and Transport. *Environ. Sci. Technol.* **2015**, *49* (9), 5663–

5671. https://doi.org/10.1021/es506245y.
(17) Shan, Y.; Harms, H.; Wick, L. Y. Electric Field Effects on Bacterial Deposition and Transport in Porous Media. *Environ. Sci. Technol.* **2018**, *52* (24), 14294–14301. https://doi.org/10.1021/acs.est.8b03648.
(18) Wick, L. Y.; Mattle, P. A.; Wattiau, P.; Harms, H. Electrokinetic Transport of PAH-Degrading Bacteria in Model Aquifers and Soil. *Environ. Sci. Technol.* **2004**, *38* (17), 4596–4602. https://doi.org/10.1021/es0354420.
(19) Gill, R. T.; Harbottle, M. J.; Smith, J. W. N.; Thornton, S. F. Electrokinetic-Enhanced Bioremediation of Organic Contaminants: A Review of Processes and Environmental Applications. *Chemosphere* **2014**, *107*, 31–42. https://doi.org/10.1016/J.CHEMOSPHERE.2014.03.019.
(20) Tatti, F.; Papini, M. P.; Raboni, M.; Viotti, P. Image Analysis Procedure for Studying Back-Diffusion Phenomena from Low-Permeability Layers in Laboratory Tests. *Sci. Rep.* **2016**, *6* (July), 1–11. https://doi.org/10.1038/srep30400.
(21) Chapman, S. W.; Parker, B. L. Plume Persistence Due to Aquitard Back Diffusion Following Dense Nonaqueous Phase Liquid Source Removal or Isolation. *Water Resour. Res.* **2005**, *41* (12). https://doi.org/10.1029/2005WR004224.
(22) Sethi, R.; Molfetta, A. Di. *Groundwater Engineering - A Technical Approach to Hydrogeology, Contaminant Transport and Groundwater Remediation*; Springer, 2019. https://doi.org/10.1016/0309-1708(88)90011-5.
(23) Pamukcu, S. In Situ Soil and Sediment Remediation: Electrokinetic and Electrochemical Methods. In *Handbook of Environmental Engineering*; Wiley Online Library, 2018; pp 209–248.
(24) Hodges, D.; Fourie, A.; Thomas, D.; Reynolds, D. Overcoming Permanganate Stalling during Electromigration. *J. Environ. Eng.* **2013**, *139* (5), 677–684. https://doi.org/10.1061/(ASCE)EE.1943-7870.0000660.
(25) Reynolds, D. A.; Jones, E. H.; Gillen, M.; Yusoff, I.; Thomas, D. G. Electrokinetic Migration of Permanganate through Low-Permeability Media. *Ground Water* **2008**, *46* (4), 629–637. https://doi.org/10.1111/j.1745-6584.2008.00415.x.
(26) Chowdhury, A. I. A.; Gerhard, J. I.; Reynolds, D.; Sleep, B. E.; O'Carroll, D. M. Electrokinetic-Enhanced Permanganate Delivery and Remediation of Contaminated Low Permeability Porous Media. *Water Res.* **2017**, *113*, 215–222. https://doi.org/10.1016/j.watres.2017.02.005.
(27) Poulson, S. R.; Naraoka, H. Carbon Isotope Fractionation during Permanganate Oxidation of Chlorinated Ethylenes (CDCE, TCE, PCE). *Environ. Sci. Technol.* **2002**, *36* (15), 3290–3274. https://doi.org/10.1021/es0205380.
(28) Newman, J.; Thomas-Alyea, K. E. *Electrochemical Systems*; John Wiley & Sons, 2004.
(29) Sprocati, R.; Rolle, M. Charge Interactions, Reaction Kinetics and Dimensionality Effects on Electrokinetic Remediation: A Model-Based Analysis. *J. Contam. Hydrol.* **2020**, *229*, 103567. https://doi.org/10.1016/j.jconhyd.2019.103567.
(30) Rasouli, P.; Steefel, C. I.; Mayer, K. U.; Rolle, M. Benchmarks for Multicomponent Diffusion and Electrochemical Migration. *Comput. Geosci.* **2015**, *19* (3), 523–533. https://doi.org/10.1007/s10596-015-9481-z.
(31) Zhang, L.; Wang, M. Modeling of Electrokinetic Reactive Transport in Micropore Using a Coupled Lattice Boltzmann Method. *J. Geophys. Res. Solid Earth* **2015**, *120* (5), 2877–2890. https://doi.org/10.1002/2014JB011812.
(32) Wang, M.; Kang, Q.; Mukherjee, P. P.; Lichtner, P. C. Mesoscopic Modeling of Multiphysicochemical Transport Phenomena in Porous Media. *Adv. Mech. Eng.* **2010**, *2*. https://doi.org/10.1155/2010/142879.

(33) Yang, Y.; Wang, M. Cation Diffusion in Compacted Clay: A Pore-Scale View. *Environ. Sci. Technol.* **2019**, *53* (4), 1976–1984. https://doi.org/10.1021/acs.est.8b05755.
(34) MacGillivray, A. D. Nernst-Planck Equations and the Electroneutrality and Donnan Equilibrium Assumptions. *J. Chem. Phys.* **1968**, *48* (7), 2903–2907. https://doi.org/10.1063/1.1669549.
(35) Sastre, M.; Santaballa, J. A. A Note on the Meaning of the Electroneutrality Condition for Solutions. *J. Chem. Educ.* **1989**, *66* (5), 403. https://doi.org/10.1021/ed066p403.
(36) Rolle, M.; Sprocati, R.; Masi, M.; Jin, B.; Muniruzzaman, M. Nernst-Planck-Based Description of Transport, Coulombic Interactions, and Geochemical Reactions in Porous Media: Modeling Approach and Benchmark Experiments. *Water Resour. Res.* **2018**, *54* (4), 3176–3195. https://doi.org/10.1002/2017WR022344.
(37) Sprocati, R.; Masi, M.; Muniruzzaman, M.; Rolle, M. Modeling Electrokinetic Transport and Biogeochemical Reactions in Porous Media: A Multidimensional Nernst-Planck-Poisson Approach with PHREEQC Coupling. *Adv. Water Resour.* **2019**, *127*, 134–147. https://doi.org/10.1016/j.advwatres.2019.03.011.
(38) Parkhurst, D. L.; Wissmeier, L. PhreeqcRM: A Reaction Module for Transport Simulators Based on the Geochemical Model PHREEQC. *Adv. Water Resour.* **2015**, *83*, 176–189. https://doi.org/10.1016/j.advwatres.2015.06.001.
(39) Sprocati, R.; Flyvbjerg, J.; Tuxen, N.; Rolle, M. Process-Based Modeling of Electrokinetic-Enhanced Bioremediation of Chlorinated Ethenes. *J. Hazard. Mater.* **2020**, *397*, 122787. https://doi.org/10.1016/j.jhazmat.2020.122787.
(40) Bear, J. *Dynamics of Fluids in Porous Media*; American Elsevier Publishing Company, 1972. https://doi.org/10.1097/00010694-197508000-00022.
(41) Hochstetler, D. L.; Rolle, M.; Chiogna, G.; Haberer, C. M.; Grathwohl, P.; Kitanidis, P. K. Effects of Compound-Specific Transverse Mixing on Steady-State Reactive Plumes: Insights from Pore-Scale Simulations and Darcy-Scale Experiments. *Adv. Water Resour.* **2013**, *54*, 1–10. https://doi.org/10.1016/j.advwatres.2012.12.007.
(42) Dentz, M.; Le Borgne, T.; Englert, A.; Bijeljic, B. Mixing, Spreading and Reaction in Heterogeneous Media: A Brief Review. *J. Contam. Hydrol.* **2011**, *120*, 1–17. https://doi.org/10.1016/j.jconhyd.2010.05.002.
(43) Kitanidis, P. K. Analysis of Macrodispersion through Volume-Averaging: Moment Equations. *Stoch. Hydrol. Hydraul.* **1992**, *6* (1), 5–25. https://doi.org/10.1007/BF01581672.
(44) Kitanidis, P. K. The Concept of the Dilution Index. *Water Resour. Res.* **1994**, *30* (7), 2011–2026. https://doi.org/10.1029/94WR00762.
(45) Rolle, M.; Kitanidis, P. K. Effects of Compound-Specific Dilution on Transient Transport and Solute Breakthrough: A Pore-Scale Analysis. *Adv. Water Resour.* **2014**, *71*, 186–199. https://doi.org/10.1016/j.advwatres.2014.06.012.
(46) Mao, X.; Wang, J.; Ciblak, A.; Cox, E. E.; Riis, C.; Terkelsen, M.; Gent, D. B.; Alshawabkeh, A. N. Electrokinetic-Enhanced Bioaugmentation for Remediation of Chlorinated Solvents Contaminated Clay. *J. Hazard. Mater.* **2012**. https://doi.org/10.1016/j.jhazmat.2012.02.001.
(47) Gill, R. T.; Thornton, S. F.; Harbottle, M. J.; Smith, J. W. Effect of Physical Heterogeneity on the Electromigration of Nitrate in Layered Granular Porous Media. *Electrochim. Acta* **2016**, *199*, 59–69. https://doi.org/10.1016/j.electacta.2016.02.191.
(48) Schmidt, C. A. B.; Barbosa, M. C.; de Almeida, M. de S. S. A Laboratory Feasibility Study on Electrokinetic Injection of Nutrients on an Organic, Tropical, Clayey Soil. *J. Hazard. Mater.* **2007**, *143* (3), 665–661. https://doi.org/10.1016/j.jhazmat.2007.01.009.

(49) Chowdhury, A. I. A.; Gerhard, J. I.; Reynolds, D.; O'Carroll, D. M. Low Permeability Zone Remediation via Oxidant Delivered by Electrokinetics and Activated by Electrical Resistance Heating: Proof of Concept. *Environ. Sci. Technol.* **2017**, *51* (22), 13295–13303. https://doi.org/10.1021/acs.est.7b02231.
(50) Wu, M. Z.; Reynolds, D. A.; Fourie, A.; Prommer, H.; Thomas, D. G. Electrokinetic in Situ Oxidation Remediation: Assessment of Parameter Sensitivities and the Influence of Aquifer Heterogeneity on Remediation Efficiency. *J. Contam. Hydrol.* **2012**, *136–137*, 72–85. https://doi.org/10.1016/j.jconhyd.2012.04.005.
(51) Fan, G.; Cang, L.; Gomes, H. I.; Zhou, D. Electrokinetic Delivery of Persulfate to Remediate PCBs Polluted Soils: Effect of Different Activation Methods. *Chemosphere* **2016**, *144*, 138–147. https://doi.org/10.1016/j.chemosphere.2015.08.074.
(52) Head, N. A.; Gerhard, J. I.; Inglis, A. M.; Nunez Garcia, A.; Chowdhury, A. I. A.; Reynolds, D. A.; de Boer, C. V.; Sidebottom, A.; Austrins, L. M.; Eimers, J.; O'Carroll, D. M. Field Test of Electrokinetically-Delivered Thermally Activated Persulfate for Remediation of Chlorinated Solvents in Clay. *Water Res.* **2020**, *183* (15), 116061. https://doi.org/10.1016/j.watres.2020.116061.
(53) Rolle, M.; Chiogna, G.; Hochstetler, D. L.; Kitanidis, P. K. On the Importance of Diffusion and Compound-Specific Mixing for Groundwater Transport: An Investigation from Pore to Field Scale. *J. Contam. Hydrol.* **2013**, *153*, 51–68. https://doi.org/10.1016/j.jconhyd.2013.07.006.
(54) Velimirovic, M.; Bianco, C.; Ferrantello, N.; Tosco, T.; Casasso, A.; Sethi, R.; Schmid, D.; Wagner, S.; Miyajima, K.; Klaas, N.; Meckenstock, R. U.; von der Kammer, F.; Hofmann, T. A Large-Scale 3D Study on Transport of Humic Acid-Coated Goethite Nanoparticles for Aquifer Remediation. *Water* **2020**, *12* (4), 1207. https://doi.org/10.3390/W12041207.
(55) Czinnerová, M.; Vološčuková, O.; Marková, K.; Ševců, A.; Černík, M.; Nosek, J. Combining Nanoscale Zero-Valent Iron with Electrokinetic Treatment for Remediation of Chlorinated Ethenes and Promoting Biodegradation: A Long-Term Field Study. *Water Res.* **2020**, *175* (15), 115692. https://doi.org/10.1016/j.watres.2020.115692.